Estimation of Unsaturated Flow Parameters by Inverse Modeling and GPR Tomography

Mohammad Bagher Farmani

Ph.D. Thesis
Oslo 2007

Department of Geosciences
Faculty of Mathematics and Natural Sciences
University of Oslo

Series of dissertations submitted to the
Faculty of Mathematics and Natural Sciences, University of Oslo
Nr. 692

ISSN 1501-7710

Cover: Inger Sandved Anfinsen.
Printed in Norway: AiT e-dit AS, Oslo, 2008.

Produced in co-operation with Unipub AS.
The thesis is produced by Unipub AS merely in connection with the
thesis defence. Kindly direct all inquiries regarding the thesis to the copyright
holder or the unit which grants the doctorate.

Unipub AS is owned by
The University Foundation for Student Life (SiO)

ABSTRACT

Estimation of flow parameters and geological structure is of fundamental importance for the modeling and understanding of hydrological processes in the subsurface. Of fundamental importance is the unsaturated zone, also called vadose zone. This zone is important in aspects of agriculture, climate changing and remediation. We use hydrological and geophysical methods to study this zone. In this study, a method is presented to estimate the flow parameters and calibrate the geological structure of the vadose zone, by conditioning the flow model on spatially continuous volumetric soil water content obtained at various times and/or groundwater table. The vadose zone at Moreppen field site located near Oslo's Gardermoen airport is used as the case study. Since snowmelt is the main groundwater recharge at Gardermoen, this study is focused on the water flow through the vadose zone during the snowmelt. Cross-well Ground Penetrating Radar (GPR) tomography method is used to estimate the spatially continuous volumetric soil water content.

Cross well GPR data sets were collected before, during and after snowmelt in 2005. The observed travel times are inverted using curved ray travel time tomography. The tomograms are in good agreement with the local geological structure of the delta. The tomographic results are confirmed independently by surface GPR reflection data and X-ray images of core samples. In addition to structure, the GPR tomograms also show a strong time dependency due to the snowmelt. The time lapse tomograms are used to estimate volumetric soil water content using Topp's equation. The volumetric soil water content is also observed independently by using a neutron meter. Comparison of these two methods reveals a strong irregular wetting process during the snowmelt. This is interpreted to be due to soil heterogeneity as well as a heterogeneous infiltration rate. The geological structure and water content estimates obtained from the GPR tomography are used in the inverse flow modeling. The water balance in the vadose zone is calculated using snow accumulation data, precipitation data, porosity estimates and observed changes in the groundwater table. The amount of water stored in the vadose zone obtained from the water balance is consistent with the amount estimated using GPR tomography.

Flow parameters and geological structure in the vadose zone are estimated by conditioning the inverse flow modeling on GPR volumetric soil water content estimates.

The influence of the tomographic artifacts on the flow inversion is minimized by assigning weights that are proportional to the ray coverage. Our flow inversion algorithm estimates the flow parameters and calibrates the geological structure. The geological structure is defined using a set of control points, the positions of which can be modified during the inversion. After the inversion, the final geological and flow model are used to compute GPR travel times to check the consistency between these computed travel times and the observed travel times. The method is first tested on two synthetic models (a steady state and a transient flow models). Subsequently, the method is applied to characterize the vadose zone near Oslo's Gardermoen Airport, in Norway, during the snowmelt in 2005. The flow inversion method is applied to locate and quantify the main geological layers at the site. In particular the inversion method identifies and estimates the location and properties of thin dipping layers with relatively low permeability. The flow model is cross validated using an independent infiltration event.

The method described above is validated using another dataset collected at the field site during the snowmelt in 2006. This time, the inverse flow modeling is performed four times and conditioned on the various datasets as follows: 1- Conditioned on time-lapse GPR travel time tomography; 2- Conditioned on groundwater table depths; 3- Conditioned on both time-lapse GPR travel time tomography and groundwater table depths: 4- Similar to inversion #2, but with using an extended search space for the intrinsic permeability and van Genuchten parameter α.

The flow parameters estimated by inversion #1 are able to capture the wet front at the correct time, but fail to simulate the groundwater table depth. The flow parameters estimated by inversion #2 fail to capture the wet front at the correct time, but decrease the objective function better than inversion #1. When the inversion is conditioned on both types of data, the final estimates of the flow parameters are very close to the estimates from the inversion conditioned on the groundwater table data only. This is because the moving groundwater table was given higher weights in the objective function as the groundwater table was monitored continuously in time while the GPR data were sampled only three times during the infiltration event. Finally we do forward flow modeling with the estimated parameter sets and compare the results with an independent tracer experiment performed at the field site in 1999. The results show that anisotropy of the intrinsic permeability is an important parameter which should be taken into account in the flow simulation. However, volumetric soil water content distribution is not strongly related

to the anisotropy of intrinsic permeability. Therefore, anisotropy can not be correctly estimated by inverse flow modeling conditioned on volumetric soil water content only.

ACKNOWLEDGMENTS

The thesis “Estimation of unsaturated flow parameters by inverse flow modeling and GPR tomography” was submitted to Department of Geosciences, University of Oslo as a requirement for the PhD degree. This work was done in collaboration with Norwegian Geotechnical Institute (NGI), Bioforsk and the Norwegian Water Resources and Energy Directorate (NVE).

Through every stage of this work I have been lucky to have had the full support from my supervisors Nils-Otto Kitterød, Henk Keers and Per Aagaard. I would like to gratefully thank Nils-Otto Kitterød for his advices during this work. I appreciate not only his full scientific support, but also his social support during my PhD studies in Norway. I thank Henk Keers for his constructive support during all stages of this work and for his ray tracing and tomography codes. Many thanks to Per Aagaard for his technical and financial support.

Special thanks to Eric Winther, Nils-Otto Kitterød and Henk Keers for their help in the field. Field work was not possible without their help, especially that of Eric Winther. I would like to thank Fan-Nian Kong at NGI for his advice and letting us use NGI’s step-frequency radar. Also many thanks to Pawel Jankowski and Harald Westerdahl, both from NGI.

I enjoyed my time in Norway especially when I was sharing it with my colleagues You Jia, Martin Morawietz, Anne Fleig, Christian Weidge, Pengxin Zhang and all other which I had contact with. Also many thanks to my very good friends Nima Hajiri, Eric Winther, Mehdi Zare, Shahab Sharifzadeh, Arash Zakeri, Hirad Nadim, Ala Abu-Ghasem and Amr Gamil. I would like to also thank Nils-Otto Kitterød’s family to be like my own family during my PhD.

Finally, I very much thank Miona Abe. Without her support, I would not have been able to finish this work and I thank my family who have always been supportive.

CONTENTS

1 MOTIVATION AND OBJECTIVES

The main goal of this work was to evaluate the possibility of estimating the flow parameters and geological structure of the unsaturated zone, also called vadose zone, using both geophysical and hydrological data and methods. The vadose zone at Moreppen field site located near Oslo's Gardermoen airport was used as the case study. Moreppen field site has been the subject of numerous studies related to sedimentological, hydrological, geophysical and geochemical processes in the saturated and vadose zone. However, in the field of hydrology none of the previous studies at Moreppen used spatially continuous geophysical data to estimate the flow parameters at the field site. In this study, cross well GPR travel time tomography for the first time was used at Moreppen to map the spatial and temporal distribution of the electromagnetic (EM) wave velocity at the field site. The EM wave velocities were converted to the soil water content using a petrophysical relationship. Then using an inverse flow modeling conditioned on volumetric soil water content, we estimated hydrological parameters in the field site. Since snowmelt is the main groundwater recharge at Gardermoen, we focused our study to the water flow through the vadose zone during the snowmelt.

In the first paper, the tomographic inversion algorithm used in this study is described. After this, the quality of the tomograms is cross validated by comparing the images with the core samples and surface GPR reflection profile. The EM wave velocities are converted to volumetric soil water content using a petrophysical relationship. The soil water content estimates are cross validated by using independent neutronmeter readings and water balance computation. These soil water content estimates are used as the conditioning data to estimate the flow parameters at the field scale. This is described in the second paper. In the first paper, we also show that cross well GPR soil water content estimates are accurate enough to be used as a known parameter in a water balance computation.

In the second paper, we present a new methodology to estimate the flow parameters in the field site conditioned on time lapse soil water content estimates derived from the tomograms. We define an objective function to minimize the differences between observed and computed soil water content estimates. By using weights in the objective function, we force the flow model to simulate the areas of the tomograms with less artifacts better than the other areas of the tomograms. These weights are determined by using the ray coverage

in the tomographic cells. In addition to the flow parameters, we also calibrate the geological structure of the flow model during the inversion. The geometry of the flow model is not fixed during the inversion. It is defined using individual and/or different sets of control points. The location of these control points can change during the inversion.

In the third paper we condition the flow inversion not only on the GPR volumetric soil water content estimates, but also on the groundwater table depth. In addition, we perform an inversion conditioned on only GPR volumetric soil water content estimates or on only the groundwater table depth to investigate if any improvements in the estimation of the flow parameters can be made when these two types of data are simultaneously used in the inversion. Finally after all inversions are finished, we do forward modeling with the estimated parameter sets and compare the results with an independent tracer experiment performed at the field site in 1999.

In the next chapter, a literature review of the hydrogeophysics related to this study is presented. After that, the theories of the applied methods are presented in detail. Then, future outlook, references, summary of the papers, and papers are presented in separate chapters, respectively.

2 LITERATURE REVIEW

2-1 Introduction to hydrogeophysics

Hydrogeophysics is a term which is used for application of geophysics in hydrology. It can be considered to be a part of shallow geophysics. The shallow subsurface is an important zone of the earth since it keeps an important part of the earth drinkable water resources. This zone is also very important in other aspects such as contaminant transport, climate changing and agriculture.

Traditionally, the shallow subsurface is studied using conventional monitoring or sampling techniques such as taking core samples and performing hydrological measurements. However, these methods are usually invasive, time-consuming and non-continuous. An alternative method for these kinds of measurements is applied geophysics (Rubin and Hubbard, 2005). Geophysical methods are usually used to map the anomalies in different disciplines such as mining and petroleum. However, in the field of hydrogeophysics, geophysical methods are used to provide quantitative information about the hydrological processes and parameters of the subsurface. This is the main challenge in hydrogeophysics.

Geophysical methods have traditionally been used in the field of hydrology to map the bedrock, to find the interface between freshwater and saltwater, to check the water quality, mapping water table and estimating and monitoring of water content (Rubin and Hubbard, 2005). More recently, geophysical and hydrological methods have been used jointly to estimate hydrological parameters (*e.g.* Lambot et al., 2004; Kowalsky et al., 2004; Kowalsky et al., 2005; Linde et al., 2006). Especially, ground penetrating radar (GPR) and electrical resistivity have been widely used in these more recent studies. A thorough review of various GPR methods used to determine soil water content has been given by Huisman *et al.* (2003) and Annan (2005). This is the method we use in this study.

2-2 Application of surface GPR reflection method in hydrology

Surface GPR reflection data are usually used in hydrology to identify the shallow subsurface geological structures. However, reflection data have also been used in some studies to derive other hydrological parameters of interest. Hubbard et al. (2002) mapped

the volumetric soil water content of a California vineyard using high-frequency GPR ground wave data. Ground wave is the direct wave between the source and receiver antennas. Huisman *et al.* (2003) compared the capability of GPR and time domain reflectometry (TDR) to assess the temporal development of spatial variation of surface volumetric soil water content by creating a heterogeneous pattern of water content using irrigation. In the case of GPR they also used ground wave data. Using geostatistical analysis of the data, they concluded that GPR is a better tool to map the soil surface water content rather than TDR.

Greaves et al. (1996) showed that when GPR data are collected with the common midpoint (CMP) multi offset geometry, stacking increases the signal-to-noise ratio of subsurface radar reflections and results in an improved subsurface image. In addition they used the normal moveout velocities, derived in the CMP velocity analysis, to estimate the water content in the subsurface. Causse and Senechal (2006) used a model based approach for the surface GPR data to build accurate travel time approximation that take into account the vertical velocity heterogeneities of the medium. They used their velocity estimates to map the volumetric soil water content in an alluvial plain using Topp's model and cross validated their estimates with other independent data such as precipitation, groundwater table and core samples. Bradford (2006) applied reflection tomography on surface reflection data to map the velocity of the EM wave in a contaminated site in USA.

Lambot *et al.* (2006) investigated the effect of soil roughness on the inversion of GPR signal for quantification of soil properties and concluded that radar signal and inversely estimated soil parameters are not significantly affected if the surface protuberances are smaller than one eighth of the wavelet.

2-3 Application of GPR and seismic tomography in hydrology

GPR tomography is the method used in this study. Therefore, the literature review related to GPR and seismic tomography is described in this separate section. In addition to GPR tomography, we also refer to seismic tomography, because they are very similar. GPR and seismic tomography have been used in hydrology for characterization of the subsurface, for the monitoring of hydrological events, for estimating the flow parameters *etc*. One of the main applications of tomography in hydrology is the delineation of the geological structure. Eppstein and Dougherty (1998) used cross well GPR data to estimate the number

of zones, their geometries and EM wave velocity within each zone before and after a controlled release of salt water in the unsaturated zone at a Vermont test site. Musil *et al.* (2003) introduced an approach to find a cave filled of air and/or water using a joint tomographic inversion of cross well seismic and GPR data. Tronicke et al. (2004) combined cross well GPR velocity tomography and attenuation tomography to characterize heterogeneous alluvial aquifers. They used multivariate statistical cluster analysis to correlate and integrate information contained in velocity and attenuation tomograms to derive the geological structure and porosity of the aquifer.

Another well established application of tomography in hydrology is the mapping and monitoring of water content in the shallow subsurface. Hubbard et al. (1997) used GPR tomography to estimate the volumetric soil water content in the unsaturated zone at the Oyster field site in Virginia, USA which consists of unconsolidated gravelly sand sediments. Furthermore, they used GPR tomography to find the preferential flow paths in the near surface fractured basalts in Idaho. Binley *et al.* (2001) monitored the water flow in unsaturated sandstone due to controlled water tracer injection using time lapse GPR travel time tomography. The time series of inferred moisture contents showed wetting and drying fronts migrating at a rate of approximately 2m per month through the sandstone. In another paper, Binley *et al.* (2002) monitored seasonal variation of moisture content in the same unsaturated sandstone caused by natural infiltration using cross well GPR and resistivity profiles. In their study GPR and resistivity tomograms showed a significant correlation. Their previous estimation of the travel times of wetting and drying fronts through the sandstone, *i.e.* 2 m per month, was again confirmed by this study.

Parkin *et al.* (2000) used cross well tomography to measure volumetric soil water content below a waste water trench. They compared the GPR estimates with neutronmeter estimates installed through the bottom of the trench and found both estimates consistent. Alumbaugh *et al.* (2002) estimated volumetric soil water content in the vadose zone before and after infiltration in a controlled field site using cross well GPR. They derived a simple site specific relationship between dielectric permittivity and volumetric soil water content to convert the velocity tomograms to the volumetric soil water content. Their estimates were fairly consistent to neutronmeter derived values with root mean square error of 2.0-3.1% volumetric soil water content between the two sets. Schmalholz *et al.* (2004) performed a time-lapse GPR tomography in a lysimeter to investigate the temporal changes and spatial distribution of the volumetric soil water content after a short but intensive

irrigation of part of the lysimeter. In their study, GPR tomography clearly showed the areas of increased water content associated with the irrigation. Hanafy and Hagrey (2006) used GPR tomography to study the subsurface distribution of tree roots using their high water content concentration property.

Tomography like any other method has its, limitations, which result in errors in the tomographic images. Like any other imaging method, the resolution of the tomographic image is usually less than the resolution of the problem under study. Alumbaugh et al. (2002) showed that a better spatial resolution of the tomograms can be obtained if data are acquired with denser source and receiver spacing. However, reducing the spacing increases the acquisition time which may be impractical because of the cost increases, resource limitations, or because subsurface changes during the time of survey. Another limitation of the acquisition geometry, which also causes errors in the tomographic images, is related to the angle between source and receiver antennas. In theory, to obtain tomographic images with the highest possible resolution from GPR data, raypaths covering a wide range of angles are required. In practice, however, the inclusion of high angle ray data in tomography inversion often leads to tomograms strongly dominated by inversion artifacts. Irving and Knight (2005) discussed the problems that arise from the standard assumption that all first arrival signals travel directly between the centers of the antennas. They showed that this assumption is often incorrect at high source-receiver angles and can lead to significant errors in tomograms when the antenna length is a significant fraction of the distance between the wells. On the other hand, if the distance between wells increases, usually the air wave is the first arrival signal at the high source-receiver angles which is not usually taken into account in most of the tomography algorithms.

In tomography, it is usually assumed that raypaths between the source and receiver antennas are straight. This assumption is correct when the medium can be considered more or less homogenous. A more precise way of finding the raypaths between the source and receiver antennas is by doing ray tracing. In ray tracing, rays bend, if necessary, to travel in the minimum time from the source antenna to the receiver antenna. However, ray equations do not take reflections and refractions into account. When there are sharp interface(s) in the medium, reflected or refracted waves may be the first arrival signals. In this case generated tomographic images contain artifacts due to assigning the wrong raypaths to the reflected or refracted waves. It is possible to take the reflected and refracted waves into account for determining the raypaths. For example Rucker and Ferre (2004)

established criteria that can be used to identify first arriving critically refracted waves from travel time profiles for cross well zero offset profiling. Hammon *et al.* (2003) used critically refracted waves as well as the reflected waves in the tomographic inversion. However, in this study we avoid the problem of facing critically refracted air waves, which are usually the first arriving signals at the shallowest part of the subsurface, by not using the cross well data near the surface. Also we assume that our vadose zone is smoothly heterogeneous because of the capillary forces and no reflection or refraction occurs at interfaces.

In cross well surveys, it is usually assumed that data sets are collected quickly relative to the temporal changes of the velocity or attenuation. However, such snapshot tomograms may contain large errors if the imaged property changes significantly during data collection. One possible solution is acquisition of less data over a shorter time. However, collecting less data usually leads to have a less resolution. Day-Lewis *et al.* (2002) proposed a sequential approach for time-lapse tomographic inversion which uses space-time parameterization and regularization to combine data collected at multiple times and to account for temporal variation.

Day-Lewis and Lane (2004) showed through a synthetic example that GPR travel time tomographic resolution varies spatially due to acquisition geometry, regularization, data error and the physics underlying the geophysical measurements. Therefore, the use of petrophysical models to convert the GPR tomograms to quantitative estimates of hydrogeological, mechanical or geochemical parameters should be performed with caution. Day-Lewis *et al.* (2005) extended the previous work and addressed the same problem for electrical resistivity tomograms.

Moysey *et al.* (2005) addressed the scale differences between the scales of derived petrophysical relationships and field scales. They introduced a numerical method which can be used to infer field scale petrophysical relationships using core scale petrophysical relationship.

2-4 Inverse flow modeling conditioned on geophysical data

Inverse flow modeling is a method to estimate the flow parameters based on some available spatial and/or temporal direct or indirect measurements. In this method, first, a forward flow model is built based on the prior information. Then, this forward flow model

is used to predict the measurements at the same positions and times. By minimizing the difference between the observed and predicted measurements, the flow parameters can be estimated.

Application of geophysical data to condition the flow inversion has been recently increased because of the extensive spatial coverage offered by geophysical methods and their ability to sample the subsurface in a minimally invasive manner. Through the different geophysical methods, GPR and resistivity are the most used ones in the inverse flow modeling. A review of different techniques to estimate the hydrological parameters using geophysical data is given by Hubbard and Rubin (2000).

Geophysical data have been used in inverse flow modeling for different purposes and in different ways. Kitterød and Finsterle (2004) used surface GPR reflection profiles to define the geometry of the flow model and measurements of water saturation in flow inversion. Hyndman et al. (1994) combined synthetic seismic and tracer data to estimate the geological structure, the effective hydraulic conductivity and seismic velocities of geological zones using a zonation algorithm. Hyndman and Gorelick (1996) developed the work done by Hyndman *et al.* (1994) and used cross well seismic, hydraulic and tracer data to estimate the three-dimensional zonation of Kesterson aquifer properties in California, USA along with the hydraulic properties as well as the seismic velocities for these zones. Linde *et al.* (2006a) did inverse flow modeling of tracer test data using GPR tomographic constraints. In another paper, Linde *et al.* (2006b) demonstrated that hydrogeological parameters can be better characterized using joint inversion of cross well electrical resistivity and GPR travel time data rather than individual inversions.

Kowalsky *et al.* (2005) estimated the soil flow parameters as well as the petrophysical parameters with the joint use of time-lapse GPR travel times and neutron meter data. Lambot *et al.* (2004) combined electromagnetic inversion of GPR signals with inverse flow modeling to estimate the flow parameters of a type of sand in laboratory condition. Binley *et al.* (2002) estimated saturated hydraulic conductivity of Sherwood sandstone by comparing the flow model results with the GPR and resistivity images.

One of the main problems in inversion algorithms, and therefore also inverse flow modeling, is equifinality (or non uniqueness). For example Binley and Beven (2003) estimated flow parameters using a natural recharge to a sandstone aquifer using 1D flow modeling. They reported a significant degree of equifinality when the flow simulations were compared to the geophysical data. To minimize this problem it is important to

constrain the inversion to the expected parameter range for example by using available *a priori* information.

3 THEORY

3-1 Cross well GPR tomography

Cross-well GPR tomography consist of two main steps: forward modeling and tomographic inversion. In the forward modeling the EM travel time from a source antenna to a receiver antenna is computed. This can be done by solving Maxwell's equations, eikonal equation or ray tracing. Rays are the orthogonal trajectories to the wavefront. Ray tracing is used to find the ray path from a source antenna to a receiver antenna. If the medium is homogeneous, rays are straight lines and inversion method is called straight ray tomography. In this method it is assumed that heterogeneity is weak in the media and straight ray paths are the good approximations of the real ray paths. This is the assumption which has been used widely in hydrogeophysics. However, in some cases heterogeneity is significant and using straight ray paths introduces artifacts which may cover the real structures that are important for flow modeling. On the other hand, in a heterogeneous medium ray paths are not straight and a way to calculate the ray trajectories is to solve the ray equations (see equations 21-22). In our case, velocity of EM waves varied up to 40% and applying straight ray tomography was not reasonable. Therefore, ray tracing was used.

Ray equations do not take the scattering and/or refractions and reflections at interfaces into account. Therefore, they are applicable when heterogeneity in the medium is smooth. In unconsolidated sediments, where capillary forces ensure the continuity, the heterogeneity in the medium can usually be considered to be smooth. If there are some known sharp interfaces in the medium, Snell's law should be applied when rays incidence to those interfaces. However, in this work the assumption of continuity is valid.

In travel time tomography, the ray equations can be used to find travel time and ray trajectory between the two known points which are the positions of source and receiver antennas for each source-receiver configuration. This kind of problem is called boundary value problem for ray equations or is sometimes referred to as two-point ray tracing problem.

There are two methods to solve two-point ray tracing problem: shooting and bending methods (Cerveny, 2001). The shooting method, which is used in this study, fixes the source position of the ray paths, takes initial take off angle and then uses the ray equations

to find the coordinate in another end point. By perturbing the take off angle, the ray path which ends to the receiver position can be found. On the other hand, the bending method fixes both source and receiver positions and takes some initial estimates of the ray path. Then, ray path is perturbed until it satisfies the minimum travel time criterion.

3-1-1 Derivation of the ray equations from Maxwell equations

Maxwell equations in a charge free medium are (Kline and Kay, 1965):

$$\begin{aligned} &\nabla.\boldsymbol{E} = 0, \\ &\nabla.\boldsymbol{B} = 0, \\ &\nabla \times \boldsymbol{E} = -\frac{\partial \boldsymbol{B}}{\partial t}, \\ &\nabla \times \boldsymbol{B} = \mu\sigma\boldsymbol{E} + \mu\varepsilon\frac{\partial \boldsymbol{E}}{\partial t}, \end{aligned} \tag{1}$$

where $\boldsymbol{E}$ is the electric field; $\boldsymbol{B}$ is the magnetic field; μ is the magnetic permeability; σ is the conductivity; and ε is the permittivity. If we take the curl of third equation we have:

$$\nabla \times \nabla \times \boldsymbol{E} = \nabla \times -\frac{\partial \boldsymbol{B}}{\partial t} = -\frac{\partial}{\partial t}\left(\nabla \times \boldsymbol{B}\right) = -\frac{\partial}{\partial t}\left(\mu\sigma\boldsymbol{E} + \mu\varepsilon\frac{\partial \boldsymbol{E}}{\partial t}\right) = -\mu\sigma\frac{\partial \boldsymbol{E}}{\partial t} - \mu\varepsilon\frac{\partial^2 \boldsymbol{E}}{\partial t^2}\,. \tag{2}$$

According to the identity rule:

$$\nabla \times \left(\nabla \times \boldsymbol{E}\right) = -\nabla^2 \boldsymbol{E}\,. \tag{3}$$

Combining equations 1, 2 and 3 gives:

$$\nabla^2 \boldsymbol{E} = \mu\sigma\frac{\partial \boldsymbol{E}}{\partial t} + \mu\varepsilon\frac{\partial^2 \boldsymbol{E}}{\partial t^2}\,. \tag{4}$$

If we assume a perfect dielectric medium, $\sigma=0$, we have:

$$\nabla^2 \boldsymbol{E} = \mu\varepsilon \frac{\partial^2 \boldsymbol{E}}{\partial t^2} . \tag{5}$$

This is usually reasonable assumption for vadose zone since soil materials, air, and clean water have very low conductivity. Equation 5 is the vector wave equation, with propagation velocity:

$$v = \frac{1}{\sqrt{\mu\varepsilon}} . \tag{6}$$

Therefore, equation 5 can be written as:

$$\nabla^2 \boldsymbol{E}(\boldsymbol{x},t) = \frac{1}{v^2(\boldsymbol{x})} \frac{\partial^2 \boldsymbol{E}(\boldsymbol{x},t)}{\partial t^2} . \tag{7}$$

We can use a Fourier transform to transform equation 7 to the frequency domain. The Fourier transform is defined:

$$F(\omega) = \int_{-\infty}^{+\infty} f(t) e^{-i\omega t} dt , \tag{8}$$

where ω is the angular frequency; $f(t)$ is the function in time domain and $F(\omega)$ is the transformed function in the frequency domain. In the frequency domain we have:

$$\nabla^2 \boldsymbol{E}(\boldsymbol{x},\omega) = \frac{\omega^2}{v^2(\boldsymbol{x})} \boldsymbol{E}(\boldsymbol{x},\omega) . \tag{9}$$

Equation 9 is called the Helmholtz vector equation. This equation can be solved with different methods such as finite difference method, finite element method and ray theory. We use ray theory to solve equation 9. If we assume that a solution of equation 9 for any component of the electric field is in the form of:

$$E(\boldsymbol{x},\omega) = A(\boldsymbol{x})e^{i\omega T(\boldsymbol{x})}, \tag{10}$$

where $A(\boldsymbol{x})$ is called wave amplitude and $T(\boldsymbol{x})$ is called eikonal (travel time or phase). we have:

$$\begin{aligned}\nabla^2 E(\boldsymbol{x},\omega) &= \nabla^2 A(\boldsymbol{x})e^{i\omega T(\boldsymbol{x})} + i\omega\left[2\nabla A(\boldsymbol{x}).\nabla T(\boldsymbol{x}) + A(\boldsymbol{x})\nabla^2 T(\boldsymbol{x})\right]e^{i\omega T(\boldsymbol{x})} \\ &- \omega^2\left(\nabla T(\boldsymbol{x})\right)^2 A(\boldsymbol{x})e^{i\omega T(\boldsymbol{x})}.\end{aligned} \tag{11}$$

Inserting equations 10 and 11 into equation 9 gives:

$$\begin{aligned}&\nabla^2 A(\boldsymbol{x})e^{i\omega T(\boldsymbol{x})} + i\omega\left[2\nabla A(\boldsymbol{x}).\nabla T(\boldsymbol{x}) + A(\boldsymbol{x})\nabla^2 T(\boldsymbol{x})\right]e^{i\omega T(\boldsymbol{x})} \\ &- \omega^2\left(\nabla T(\boldsymbol{x})\right)^2 A(\boldsymbol{x})e^{i\omega T(\boldsymbol{x})} = \frac{\omega^2}{v^2(\boldsymbol{x})}A(\boldsymbol{x})e^{i\omega T(\boldsymbol{x})}.\end{aligned} \tag{12}$$

If we rearrange the terms in this equation:

$$\frac{\nabla^2 A(\boldsymbol{x})}{\omega^2 A(\boldsymbol{x})} + i\frac{1}{\omega}\left[\frac{2\nabla A(\boldsymbol{x}).\nabla T(\boldsymbol{x})}{A(\boldsymbol{x})} + \nabla^2 T(\boldsymbol{x})\right] - \left(\nabla T(\boldsymbol{x})\right)^2 = \frac{1}{v^2(\boldsymbol{x})}. \tag{13}$$

When $\omega\rightarrow\infty$, the first and second terms on the left hand side of equation 13 converge to zero. This gives:

$$\left(\nabla T(\boldsymbol{x})\right)^2 = \frac{1}{v^2(\boldsymbol{x})}. \tag{14}$$

Equation 14 is called the eikonal equation. It describes the travel time propagation, $T(\mathbf{x})$ from the source to the point $\mathbf{x}$. This equation can be solved using finite difference method. Since this method is not used in this study, its theory is not presented here. The ray equations can be derived from the eikonal equation. This equation controls the evolution of wavefront. One disadvantage of using the eikonal equation is that we need to sample the whole medium while ray tracing will only sample a line inside the medium. Therefore, instead of computing the wavefront we can only focus on the orthogonal trajectories of wavefronts at each point which are called rays. To derive the ray equations we consider a small enough region that the rays are locally linear. If $d\mathbf{x}$ is a tangent along the ray with length of ds, then:

$$\frac{d\mathbf{x}}{ds} = \mathbf{n}\,. \tag{15}$$

where $\mathbf{n}$ is a unit vector which shows the direction of the ray. Combining equations 14 and 15 gives us

$$\nabla T = \frac{1}{v}\mathbf{n} = \frac{1}{v}\frac{d\mathbf{x}}{ds}\,, \tag{16}$$

where $\mathbf{x} = (x_1, x_2, x_3)$. For simplicity, we replaced $T(\mathbf{x})$ and $v(\mathbf{x})$ with T and v, respectively. Consider taking the gradient of the eikonal equation:

$$\nabla(\nabla T)^2 = 2\nabla T.\nabla(\nabla T) = 2\frac{1}{v}\nabla\left(\frac{1}{v}\right) \tag{17}$$

Based on the chain rule:

$$\frac{dT}{ds} = \frac{d\mathbf{x}}{ds}.\nabla T \tag{18}$$

Combining equations 16, 17 and 18:

$$\nabla\left(\frac{1}{v}\right)=\frac{d}{ds}\left[\frac{1}{v}\frac{d\boldsymbol{x}}{ds}\right]. \tag{19}$$

Equation 19 is called the second order differential equation for rays. If we transform equation 19 to first order differential equations using:

$$\boldsymbol{p}=\frac{1}{v}\frac{d\boldsymbol{x}}{ds}, \tag{20}$$

and rearranging equations 19 and 20 we end up with ray equations:

$$\begin{aligned}\frac{d\boldsymbol{x}}{ds}&=v\boldsymbol{p}\ ,\\ \frac{d\boldsymbol{p}}{ds}&=\frac{\partial}{\partial\boldsymbol{x}}\left(\frac{1}{v}\right),\end{aligned} \tag{21}$$

where $\boldsymbol{x}=(x_1(s),x_2(s),x_3(s))$ is the ray path; $\boldsymbol{p}=(p_1(s),p_2(s),p_3(s))$ is the slowness vector (tangent vector to the ray path); $v=v(\boldsymbol{x})$ is the velocity at $\boldsymbol{x}$; and the independent parameter s in equation 1 is the arc length along the ray. The initial conditions for the ray equations are $\boldsymbol{x}(0)=\boldsymbol{x}_s, \boldsymbol{p}(0)=\boldsymbol{p}_s$. In our study, $\boldsymbol{x}_s$ is the position of the source antenna, and $\boldsymbol{p}_s$ is the slowness vector at the source, i.e. the vector pointing in the direction in which the ray leaves the source antenna. In this paper the velocity values are given on square grids with a grid size of 10 on 10 cm. Travel time can be computed from equations 14, 16 and 18:

$$\frac{dT}{ds}=\frac{1}{v}\ . \tag{22}$$

The computation of a ray path from a source in one well to a receiver in another well ('two-point ray tracing' (e.g. Cerveny, 2001)), requires two steps (Keers *et al.*, 2000). First, the ray paths from a source in one well to the other well are computed with varying take-off angles. This can be carried out using various methods. In this paper we employ a fourth order variable step size Runge-Kutta method (Press *et al.*, 1992). The Runge-Kutta method is described in detail in the next sub section. The ray tracing also requires the computation of the velocity and its gradient at arbitrary points. This is done using two dimensional cubic splines (Press *et al.*, 1992).

This 'one point ray tracing' gives the positions of a discrete number of rays in the receiver well as a function of the take-off angle. Root solving can then be employed to solve the two point ray tracing problem, *i.e.* to find the take-off direction for a certain position in the receiver well. The root solving method used in this study is bisection (Press *et al.*, 1992). Newton's method may also be used. However, we found bisection already to be quite efficient. This two-point ray tracing method is particularly efficient if one has to do two point ray tracing from one source to many receivers, as in this study.

3-1-2 Runge-Kutta ordinary differential equation solver

Runge-Kutta is a method of numerically integrating ordinary differential equations by using a trial step at the midpoint of an interval to cancel out lower-order error terms. The most often used method is fourth-order Runge-Kutta formula (Press *et al.*, 1992). In this method the derivative is evaluated four times in each step: once at the initial point, twice at trial midpoints, and once at a trial endpoint (Press *et al.*, 1992). From these derivatives the final function value is calculated.

Consider a first order ordinary differential equation such as:

$$\frac{dy}{dx} = f(x, y)\,. \tag{23}$$

Given an initial condition $y(x_0)=y_0$ we choose the lag step h, the Runge-Kutta orders are defined as:

$$
\begin{aligned}
k_1 &= hf(x_n, y_n), \\
k_2 &= hf(x_n + \frac{h}{2}, y_n + \frac{k_1}{2}), \\
k_3 &= hf(x_n + \frac{h}{2}, y_n + \frac{k_2}{2}), \\
k_4 &= hf(x_n + h, y_n + k_3),
\end{aligned}
\tag{24}
$$

where n is the point index. y the value at point $n+1$ is calculated with:

$$
y_{n+1} = y_n + \frac{k_1}{6} + \frac{k_2}{3} + \frac{k_3}{3} + \frac{k_4}{6} + O(h^5), \tag{25}
$$

Where $O(h^5)$ is the error of estimation.

3-1-3 Spline interpolation

When values of a function are available in some points and the analytical expression of the function is not defined, interpolation is used to find values of the function in arbitrary points. Interpolation process have two stages: first fit an interpolating function to the data points provided in the neighborhood of the desired point and then evaluate that interpolating function at the desired point.

If continuity of the derivatives is not taken into account, linear interpolation may be used. Otherwise, some other interpolation methods should be applied which consider the continuity of the derivatives. In this work we used cubic spline interpolation. The goal of the cubic spline interpolation is to get a cubic polynomial interpolation formula that is smooth in the first derivative, and continuous in the second derivative, both within an interval and at its boundaries.

The cubic spline formula is defined as (Press *et al.*, 1992):

$$
S(x) = \begin{cases}
s_1(x) & if \quad x_1 \le x \le x_2 \\
s_2(x) & if \quad x_2 \le x \le x_3 \\
\quad\vdots & \\
s_{n-1}(x) & if \quad x_{n-1} \le x \le x_n,
\end{cases}
\tag{26}
$$

where s_i is the third degree polynomial defined by

$$s_i(x) = a_i(x-x_i)^3 + b_i(x-x_i)^2 + c_i(x-x_i) + d_i \qquad i= 1, 2, \ldots, n\text{-}1. \tag{27}$$

To find values of the coefficients in equation 27 we consider cubic spline assumptions:

1. The piecewise function *S(x)* will interpolate all data points.

2. *S(x)* will be continuous on the interval $[x_1,x_n]$.

3. *S'(x)* will be continuous on the interval $[x_1,x_n]$.

4. *S''(x)* will be continuous on the interval $[x_1,x_n]$.

If we perform substitution of $h=x_{i+1}-x_i$ and $M_i=s_i''(x_i)$ and apply above assumptions, we end up with the following equations for coefficients:

$$\begin{aligned} a_i &= \frac{M_{i+1}-M_i}{6h}, \\ b_i &= \frac{M_i}{2}, \\ c_i &= \frac{y_{i+1}-y_i}{h} - \left(\frac{M_{i+1}-2M_i}{6}\right)h, \\ d_i &= y_i. \end{aligned} \tag{28}$$

Now the problem is reduced to find the second derivatives of data points. If we use continuity for the first derivative, we will have n-2 equations to find n unknown derivatives. Therefore the system of equation is under-determined. For a unique solution we need to specify two further conditions. If we assume that the second derivative at x_1 and x_n are 0, then the system of equations is complete. This method is called natural cubic splines.

This interpolation is only one dimensional. For our purpose we need to interpolate in two dimensions, *v(x,y)*. One option is using two dimensional spline interpolation called bicubic spline interpolation. However, this method of calculation is quite complicated and time-consuming. As an alternative, we applied a simpler method which consists of two one dimensional spline interpolations instead of two dimensional spline interpolation. First *n*

one dimensional spline interpolation were performed across the rows of velocity values and velocities at [(x,y_j), $j = 1, \ldots, n$] were determined. Then, one additional one dimensional spline interpolation was performed across the newly created column $(X=x)$ and the velocity at (x,y) was determined.

3-1-4 Travel time tomography inversion

Once ray tracing is performed for a cross well survey and ray paths are determined, tomography inversion is applied to determine the velocity either in a continuous medium or in a divided medium into the homogenous cells. For each ray path in a continuous medium, travel time can be calculated from:

$$T_i = \int_{S_i} \frac{ds}{v} \qquad i = 1, \ldots, N \ , \tag{29}$$

where T_i is the travel time for ray (source-receiver combination) i; S_i is the ray path; v is the velocity; and N is the total number of source-receiver combinations. In tomography we solve equation (29) for v. In some cases, *e.g.* global seismic tomography, there is usually a good initial guess of the velocity which can be used to calculate equation 29 (Nolet, 1987). In other cases, when no information about the velocity is available, the average velocity of all source-receiver combinations may be used as the initial guess. The average velocity can be calculated by assuming straight ray paths and using observed travel times (*e.g.* recorded by GPR during acquisition). This is the initial velocity which we use in ray tracing codes to calculate travel times and find the ray paths. Because we use a homogenous background velocity as the initial velocity in ray tracing, all ray paths are straight rays for zero iteration. In other words, zero iteration gives us straight ray tomography estimations. According to the starting model the travel time is calculated by:

$$T_i^0 = \int_{S_i^0} \frac{ds}{v_0} \qquad i = 1, \ldots, N \ , \tag{30}$$

where s_i^0 is the ray path in the starting model. Now differences between observed travel times and calculated travel times can be computed by (Nolet, 1987):

$$\delta T_i = \int_{S_i} \frac{ds}{v} - \int_{S_i^0} \frac{ds}{v} \approx \int_{s_i^0} (\frac{1}{v} - \frac{1}{v_0}) ds \approx - \int_{s_i^0} \frac{\delta v}{v_0^2} ds \,, \tag{31}$$

$$\delta v = v - v_0 \,, \tag{32}$$

where δT_i is called time residual. Note that in equation 31 we assume that the initial velocity and the ray paths are close to the true velocity and true ray paths. Therefore, it is very important that the initial velocity is as close as possible to the true velocity. Equations 31 are called tomography equations. The only unknown in tomography equations is velocity, since time residuals and ray paths are determined as part of the ray tracing. Usually, we subdivide the medium into small cells. In this case, tomography equations are expressed in discrete form as:

$$\delta T_i = \sum_k - \frac{l_{ik}}{v_k^2} \delta v_k \,, \qquad i = 1,\ldots,N \quad k = 1,\ldots,M, \tag{33}$$

Here l_{ik} is the length of ray i through the velocity cell k and the starting velocity in cell k is denoted by v_k. Equation 33 can be written in matrix form as:

$$\boldsymbol{\delta T = L\, \delta V}. \tag{34}$$

For real data, the equations can be extended to account for small errors in the source and receiver locations (Keers *et al.*, 2000); this is obviously not necessary for the inversion of synthetic models. In matrix form the new system of equations can be written as:

$$\boldsymbol{\delta T} = \widetilde{\boldsymbol{L}}\boldsymbol{\delta}\widetilde{\boldsymbol{V}}\,, \tag{35}$$

where

$$\widetilde{\boldsymbol{L}} = \begin{pmatrix} \boldsymbol{L} & \boldsymbol{L_R} & \boldsymbol{L_S} \end{pmatrix},$$

$$\boldsymbol{\delta}\widetilde{\boldsymbol{V}} = \begin{pmatrix} \boldsymbol{\delta V} \\ \boldsymbol{\delta V_R} \\ \boldsymbol{\delta V_S} \end{pmatrix},$$

where $\boldsymbol{L}$ is a coefficient matrix consisting of the parameters in equation (33); $\boldsymbol{L_R}$ and $\boldsymbol{L_S}$ are the matrices of 0's and 1's depending on whether the source/receiver is active; $\boldsymbol{\delta V_R}$ and $\boldsymbol{\delta V_S}$ represent source and receiver statics. Here, statics are the time shifts associated with small errors in the source and receiver locations.

Equation 35 is usually an ill-conditioned equation. An equation is ill-conditioned if small changes in the coefficients of the solution have drastic effects on the results. To ensure physically reasonable results, this equation can be stabilized by adding two terms to minimize a combination of velocity variation (damping) and velocity gradients (smoothing). The final system of equations in the matrix form is:

$$\begin{pmatrix} \boldsymbol{\delta T} \\ \boldsymbol{0} \\ \boldsymbol{0} \end{pmatrix} = \underbrace{\begin{pmatrix} \boldsymbol{L} & \boldsymbol{L_R} & \boldsymbol{L_S} \\ \lambda_1 \boldsymbol{I} & \boldsymbol{0_R} & \boldsymbol{0_S} \\ \lambda_2 \boldsymbol{D} & \boldsymbol{0_R} & \boldsymbol{0_S} \end{pmatrix}}_{\widetilde{\widetilde{\boldsymbol{L}}}} \begin{pmatrix} \boldsymbol{\delta V} \\ \boldsymbol{\delta V_R} \\ \boldsymbol{\delta V_S} \end{pmatrix}, \tag{36}$$

where λ_1 is the damping factor; λ_2 is the smoothing parameter; $\boldsymbol{I}$ is the M by M identity matrix; $\boldsymbol{0_R}$ and $\boldsymbol{0_S}$ are zero matrices; and $\boldsymbol{D}$ is the smoothing operator. The damping parameter keeps the model close to the initial one and the smoothing parameter reduces the velocity gradient in adjacent cells. They are empirically determined scaling constants. The smoothing operator, $\boldsymbol{D}$, is a non square matrix of size $\sum n_n \times M$ given by:

$$D_{lm} = \begin{cases} 1 & m = l \\ -1 & m = desired\ neighbor\ of\ l \\ 0 & otherwise \end{cases}$$

where n_n is the number of neighbors for each cell.

In equation 36 most of the elements of matrix $\tilde{\tilde{L}}$ are zero since each ray only passes few cells from source to receiver antenna. $\tilde{\tilde{L}}$ is a sparse matrix and, therefore, it can be solved efficiently using the LSQR algorithm (Paige and Saunders, 1982). We use this algorithm to solve equation 36 iteratively. Velocities obtained in one iteration are used as the starting velocities for the next iteration. Other popular algorithms to solve equation 36 are algebraic reconstruction technique (ART) and simultaneous iterative reconstruction technique (SIRT).

3-2 Estimation of water content from velocity tomograms

The tomogram gives a spatial velocity distribution of the medium between the source and receiver wells. We apply the conventional assumption that the EM-velocity of the medium, v, is described by:

$$v \approx \frac{c_a}{\sqrt{\varepsilon}}, \tag{37}$$

where c_a is the velocity of an EM wave through the air and ε is the relative dielectric permittivity of the medium (Davis and Annan, 1989). Note that at high frequencies, the dielectric permittivity of the medium is independent of frequency and dispersion does not occur. For example West *et al.* (2003) showed that the dielectric permittivity of the Sherwood Sandstone aquifer in the UK, having different lithology from medium-grained sandstone with very little clay to fine-grained sandstone up to 5% clay, does not show dispersion in the frequency range from 350 MHz to 1000 MHz. Below 350 MHZ (down to 75 MHZ), dielectric permittivity of the clean sandstone is independent of frequency. However, clay minerals introduce dispersion for the frequencies below 350 MHz. The central frequency used in our study is 475 MHz.

The water content in the medium can be estimated from its dielectric permittivity using a soil-physics relationship. If it is applicable, it is worth to derive site specific soil-physics relationship. However, deriving this relationship is a demanding task and usually needs many precise laboratory tests on the soil samples from the site. An alternative option is using one of the widely used soil-physics relationships. Topp's model (Topp *et al.*, 1980)

and the Complex Refractive Index Model (CRIM) (Wharton *et al.*, 1980) are the most popular models to estimate volumetric soil water content from EM wave velocity. CRIM is a physical model and Topp's model is an experimental model. CRIM relates the dielectric permittivity of the medium to the dielectric permittivity of its components as:

$$\varepsilon = \left[(1-\varphi)\varepsilon_s^{\alpha} + S_w\varphi\,\varepsilon_w^{\alpha} + (1-S_w)\varphi\varepsilon_a^{\alpha}\right]^{1/\alpha}, \tag{38}$$

Here ε_a, ε_s and ε_w are the relative dielectric permittivity of air, soil material and water, respectively; φ is the porosity; α is an exponent parameter; and S_w is the water saturation which is related to volumetric soil water content by:

$$\theta = \varphi\, S_w . \tag{39}$$

α is theoretically assumed to be 0.5 for an isotropic soil (*e.g.* Alharthi and Lange, 1987). Laboratory tests performed by Yu *et al.* (1997) confirmed the value of 0.5 for isotropic soils. Roth *et al.* (1990) obtained the value of 0.46 for α in the laboratory using large soil samples from eleven different field sites. Even though CRIM is mainly based on physical assumptions and therefore, in theory, seems to be a good model to use, difficulties to measure ε_s and φ prohibited us to use it. Therefore, in this study Topp's empirical model was used. For a range of sediments (from clay to sandy loam), Topp *et al.* (1980) found a general experimental relationship between volumetric soil water content and apparent permittivity:

$$\theta = a + b\varepsilon_a + c\varepsilon_a^2 + d\varepsilon_a^3, \tag{40}$$

where

$$a = -5.3\times10^{-2}, b = 2.92\times10^{-2}, c = -5.5\times10^{-4}, d = 4.3\times10^{-6} .$$

They also introduced separate relationships for different types of soils. Since the vadose zone at our research field site consists mainly of sand, Topp's model for sandy loam was used in this study:

$a = -5.75 \times 10^{-2}, b = 3.09 \times 10^{-2}, c = -7.44 \times 10^{-4}, d = 9.634 \times 10^{-6}$.

According to Topp *et al.* (1980) the uncertainty in the values of θ in equation (5) is about σ_{Topp}= 0.0089. For low-loss materials $\varepsilon_a \approx \varepsilon$ and, therefore, θ can be determined from the velocity using equations 37 and 40. The applicability of Topp's model to sandy soil was proven by Ponizovsky *et al.* (1999).

In addition to Topp's model and CRIM, there are some other rock physics models which can potentially be used. For example Yu *et al.* (1997) introduced an empirical relationship between the dielectric permittivity and volumetric soil water content for sand using laboratory tests. However, we found that Yu's model overestimates the volumetric soil water content in our field site. Persson *et al.* (2002) used artificial neural networks to predict the relationship between dielectric permittivity and water content. Alumbaugh *et al.* (2002) derived a linear site specific relationship between volumetric soil water content and dielectric permittivity.

3-3 Forward flow modeling

Water flow in a heterogeneous variably saturated porous medium is modeled by Richards' equation (Richards, 1931; Comsol Multiphysics, 2004). Richards' equation is a non-linear partial differential equation which is obtained by combining Darcy's law and requirement for continuity of mass. To derive Richard's equation, we assume a porous medium with volume Δx, Δy and Δz in x, y and z direction, respectively (figure 1).

For this medium flow in the x, y and z direction are respectively given by:

$$\begin{aligned} q_{xin} &= v_x \Delta y \Delta z \\ q_{xout} &= (v_x + \frac{\partial v_x}{\partial x} \Delta x) \Delta y \Delta z \end{aligned} \quad , \tag{41}$$

$$\begin{aligned} q_{yin} &= v_y \Delta x \Delta z \\ q_{yout} &= (v_y + \frac{\partial v_y}{\partial y} \Delta y) \Delta x \Delta z \end{aligned} \quad , \tag{42}$$

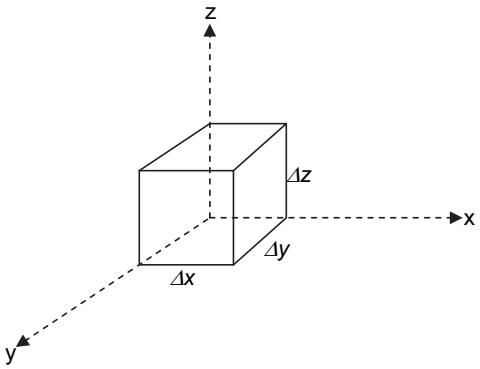

Figure 1. Porous medium

$$\begin{aligned} q_{zin} &= v_z \Delta x \Delta y \\ q_{zout} &= (v_z + \frac{\partial v_z}{\partial z} \Delta z) \Delta x \Delta y \end{aligned} \quad , \tag{43}$$

where q_{xin}, q_{yin} and q_{zin} are influx into the medium; q_{xout}, q_{yout} and q_{zout} are outflux of the medium; and v_x, v_y and v_z are velocity in x, y and z direction, respectively. From continuity of mass, we have:

$$\sum q_{in} - \sum q_{out} = \frac{\partial \theta}{\partial t} \Delta x \Delta y \Delta z \, . \tag{44}$$

If we combine equations 41 to 44 we find:

$$-\left(\frac{\partial v_x}{\partial x} + \frac{\partial v_y}{\partial y} + \frac{\partial v_z}{\partial z} \right) = \frac{\partial \theta}{\partial t} \, . \tag{45}$$

According to Darcy's law:

$$v_x = -K_x \frac{\partial h}{\partial x}$$
$$v_y = -K_y \frac{\partial h}{\partial y}, \quad (46)$$
$$v_z = -K_z \frac{\partial h}{\partial z}$$

where K is the hydraulic conductivity and h is the hydraulic head. Hydraulic conductivity is a function of the properties of the porous medium and the properties of the fluid:

$$K = \frac{k_s \rho_f g k_r}{\eta}, \quad (47)$$

$$h = \psi + z = \frac{p}{\rho_f g} + z, \quad (48)$$

where k_s is the intrinsic or absolute permeability; η *is* the fluid viscosity; k_r is the relative permeability; ρ_f is the density of water; g is the gravitational acceleration; z is the gravitational head which is positive upward; ψ is the pressure head; and p is the pressure. Now by combining equations 45 to 48, Richard's equation is derived:

$$\frac{\partial \theta}{\partial t} + \nabla . \left[-\frac{k_s}{\eta} k_r \nabla \left(p + \rho_f g z \right) \right] = 0 . \quad (49)$$

Equation 49 is not mathematically tractable because two dependent variables p and θ are present. However, by using the specific capacity function, C, one of these variables can be eliminated. The specific capacity function is defined as:

$$C = \frac{\partial \theta}{\partial p} . \quad (50)$$

If we choose p as the dependent variable and add a source or sink term, Q_s, and storage coefficient, S_s, to Richard's equation, we have:

$$[C + S_e S_s]\frac{\partial p}{\partial t} + \nabla.\left[-\frac{k_s}{\eta} k_r \nabla\left(p + \rho_f g z\right)\right] = Q_s, \tag{51}$$

where S_e is the effective saturation. S_s is related to the compression and expansion of the pore space and the water. Richards' equation is highly nonlinear in the vadose zone because θ, S_e, C, and k_r vary as a function of water saturation. For these parameters constitutive relations are needed. Two widely used constitutive relations are Brooks and Corey (Brooks and Corey, 1966) and van Genuchten (van Genuchten, 1980) relations. Brooks and Corey (1966) relations are:

$$\theta = \theta_r + S_e\left(\theta_s - \theta_r\right), \tag{52}$$

$$S_e = \left|\frac{\alpha p}{\rho_f g}\right|^{-n}, \tag{53}$$

$$C = \frac{-n\rho_f g}{p}\left(\theta_s - \theta_r\right)\left|\frac{\alpha p}{\rho_f g}\right|^{-n}, \tag{54}$$

$$k_r = s_e^{2/n+l+2}, \tag{55}$$

and van Genuchten (1980) relations are:

$$\theta = \theta_r + S_e\left(\theta_s - \theta_r\right), \tag{56}$$

$$S_e = \left(1 + \left|\frac{\alpha p}{\rho_f g}\right|^{n}\right)^{-m}, \tag{57}$$

$$C = \frac{\alpha m}{1-m}\left(\theta_s - \theta_r\right) S_e^{1/m}\left(1 - S_e^{1/m}\right)^{m}, \tag{58}$$

$$k_r = S_e^{L}\left[1 - \left(1 - S_e^{1/m}\right)^{m}\right]^{2}, \tag{59}$$

where θ_r is the residual water content; and θ_s is the maximum water content. α, m, n, and L are parameters which characterize the porous medium. In this study van Genuchten constitutive relations were used.

A unique solution of equation 51 requires boundary conditions. It also requires initial conditions for transient problems. The boundary conditions used in this study are as follows:

$$p = p_0 , \tag{60}$$

$$p = 0 , \tag{61}$$

$$\boldsymbol{n} \cdot \frac{k_s}{\eta} k_r \nabla\left(p + \rho_f g z\right) = 0 , \tag{62}$$

$$\boldsymbol{n} \cdot \frac{k_s}{\eta} k_r \nabla\left(p + \rho_f g z\right) = N_0 , \tag{63}$$

$$\boldsymbol{n} \cdot \left(\frac{k_{s1}}{\eta} k_{r1} \nabla\left(p_1 + \rho_f g z\right) - \frac{k_{s2}}{\eta} k_{r2} \nabla\left(p_2 + \rho_f g z\right) \right) = 0 , \tag{64}$$

where $\boldsymbol{n}$ is the vector normal to the boundary. Equation 60 is used to define the known distribution of pressure at boundary. For example, if the bottom boundary of the flow model is below the groundwater table, pressure is known. At groundwater table, the pressure is zero which can be defined as the boundary condition using equation 61. Zero flux across the boundary can be defined using equation 62. In this study, we define sides' boundaries of our models as impervious boundaries. If there is inward or outward flux to the model through a boundary, it can be defined using equation 63. Finally, we condition an interior boundary using equation 64 which implies the continuity across the boundary.

We solve Richards' equation using the finite element code FEMLAB3.1 (Comsol Multiphysics, 2004).

3-4 Inverse flow modeling

The theory of inverse modeling is described in a variety of textbooks for applied mathematics and mathematical statistics (e.g. Stengel, 1994; Björk, 1996). However,

because water flow in the vadose zone is a non-linear complex function of the flow parameters, formulation of the inverse problem and minimization of the objective function is still the main challenge for the hydrogeophysical community. One of the classical series of papers about implementing the inverse modeling in the field of hydrology is given by Carrera and Neuman (1986a,b,c).

The major steps of the inverse modeling of flow parameters can be summarized as follows (Finsterle, 2000):

1- Building a model which represents the hydrogeological system under test conditions (conceptual model). In this step, the geometry of the flow model, the boundary conditions and numerical method which is used to solve the Richards' equation are defined. The model should be able to capture the general features of the system of interest.

2- Selecting the parameters that should be estimated (parameters selection). In this step, we define a vector **p** of length *n* containing the flow parameters to be estimated by inverse flow modeling. This is a trade off in the inverse flow modeling. If too many parameters are defined to be estimated, then the flow model becomes large and unstable. On the other hand, if very few parameters are defined to be estimated, then the model may not be a representative model for the system of interest.

3- Selecting the initial values for the parameters (initial values). An initial guess has to be assigned to each element of **p**. This forms the vector of initial guess $\mathbf{p_0}$. The initial guess can be the prior information vector **p***. However, $\mathbf{p_0}$ and **p*** must be distinguished from each other. **p*** might also be used to constrain or regularize the inverse problem. In other words, **p*** might contribute in the objective function. It is worth to perform several inversions with different initial guesses to detect if the optimization algorithm has found the global minimum.

4- Selecting the calibration data in time and space (calibration data). The availability of high quality observed data is the key requirement for reliably estimating model parameters. Vector **z*** of length *m* holds the observed data in time and space. The observed data can be any kind of data which can be directly or indirectly calculated from the response of the flow model. However, the selected types of data should be sensitive enough to the variations of the flow parameters which are estimated. The

difference between the observed, **z***, and calculated, **z**, system response are summarized in the residual vector **r** of length *m*:

$$\mathbf{r} = \mathbf{z}^* - \mathbf{z}. \tag{65}$$

5- Assignment of weights to the calibration data (weights). The observation vector includes data that can be of different type, magnitude and accuracy. Therefore, each residual should be weighted before the value of the objective function can be calculated. In the classical inverse flow modeling, residuals are weighted with the inverse of the observation covariance matrix $\mathbf{C}_{\mathbf{zz}}$.

6- Calculation of the model (forward modeling). A simulation is performed using the current value of the parameter vector **p** to obtain the calculated system response **z**(**p**). This simulation is repeated during the inverse flow modeling with updated parameters suggested by the optimization algorithm.

7- Comparison of the calculated and observed data (objective function). The objective function, *O*, is a function which is used to mathematically measure the misfit between observed and calculated data. If a distributional assumption about the residuals is made, the objective function can be derived from maximum likelihood considerations. If residuals are normally distributed, minimizing the weighted least squares objective function leads to maximum likelihood estimates:

$$O = \sum_{i=1}^{m} \frac{r_i^2}{\sigma_{z_i}^2}. \tag{66}$$

8- Updating the parameters to obtain a better fit between calculated and observed data (optimization algorithm). Since the model output, **z**(**p**), depends on the parameters to be estimated, the fit can be improved by changing the elements of parameter vector **p**. There are different algorithms which can be used to iteratively find smaller values of the objective functions.

9- Iteration of steps 6 to 8 until no better fit can be obtained (convergence criteria). Once the decrease in the objective function is less than our criteria, the iterative optimization procedure is terminated.

10- Analysis of the residual and estimation of uncertainty (error analyses).

4 FUTURE OUTLOOK

As many other PhD works, because of limited time available and lack of further human and technical resources, many doors stayed open for further analyses and improvements. Some suggestions are presented below for future possible works:

- *Travel time tomography*: It would be useful to include anisotropy in travel time tomography. Anisotropic velocities may be used to obtain more informative data from the tomograms. Anisotropic velocity can be presented as (Watanabe *et al.*, 1996):

$$\boldsymbol{v}(\varphi) = \boldsymbol{v}^m + \boldsymbol{v}^d cos2\varphi\,, \tag{67}$$

where

$$\boldsymbol{v}^m = \frac{1}{2}\left(\boldsymbol{v}^{max} + \boldsymbol{v}^{min}\right), \tag{68}$$

$$\boldsymbol{v}^d = \frac{1}{2}\left(\boldsymbol{v}^{max} - \boldsymbol{v}^{min}\right), \tag{69}$$

$$\phi = \theta - \delta\,, \tag{70}$$

δ is the angle of maximum velocity with x axis and θ is the angle of ray with x axis. By combining equations 67 and 70 we have:

$$\boldsymbol{v}_{ray} = \boldsymbol{v}^m + \boldsymbol{v}^d cos2(\theta - \delta)\ . \tag{71}$$

This is the formula of anisotropic velocity. We subdivide the medium to small cells. The tomographic equation is:

$$\Delta T_i = \sum_k -\frac{l_{ik}}{\boldsymbol{v}_{ik}^2}\Delta \boldsymbol{v}_{ik} \quad i = 1,\ldots,N \quad k = 1,\ldots,M. \tag{72}$$

Here l_{ik} is the length of ray i through the velocity cell k and the starting velocity in cell k for each iteration is denoted by $\boldsymbol{v}_{ik}$. $\Delta\boldsymbol{v}_{ik}$ is the velocity update for each cell which can be obtained from equation 71:

$$\Delta\boldsymbol{v}_{ik} = \Delta\boldsymbol{v}_k^m + \Delta\boldsymbol{v}_k^d cos2\delta_k cos2\theta_{ik} + \Delta\boldsymbol{v}_k^d sin2\delta_k sin2\theta_{ik} \ . \tag{73}$$

Therefore, based on equations 72 and 73 the unknown parameters and their coefficients are respectively:

$$\Delta\boldsymbol{v}_k = \left(\Delta\boldsymbol{v}_k^m, \Delta\boldsymbol{v}_k^d cos2\delta_k, \Delta\boldsymbol{v}_k^d sin2\delta_k\right) \tag{74}$$

$$A_{ik} = \left(-\frac{l_{ik}}{\boldsymbol{v}_{ik}^2}, -\frac{l_{ik}}{\boldsymbol{v}_{ik}^2} cos2\theta_{ik}, -\frac{l_{ik}}{\boldsymbol{v}_{ik}^2} sin2\theta_{ik}\right) \tag{75}$$

After solving the tomographic equation, $\Delta\boldsymbol{v}^d_k$ and δ_k can simply be obtained from:

$$\Delta\boldsymbol{v}_k^d = \sqrt{\left(\Delta\boldsymbol{v}_k^d cos2\delta_k\right)^2 + \left(\Delta\boldsymbol{v}_k^d sin2\delta_k\right)^2} \tag{76}$$

$$\delta_k = \frac{1}{2} tan^{-1}\left(\frac{\Delta\boldsymbol{v}_k^d sin2\delta_k}{\Delta\boldsymbol{v}_k^d cos2\delta_k}\right) \tag{77}$$

Some attempts were done in this work to use anisotropic directions to define the geological interfaces more accurately. Even though the preliminary results were promising, more work needs to be done to develop our tomographic codes for the accurate anisotropic computations and this was left for future studies. Another thought is that it might be possible to link anisotropy in EM-velocity to anisotropy in intrinsic permeability. However, we did not do any attempt to test this possibility.

- *Error propagation analysis for the final estimates of the flow parameters from the inverse flow modeling*: Standard deviations of the final estimates of the flow parameters were

calculated with the assumption of normality and linearity. To have a better estimation of the uncertainty more advanced error propagation analysis is needed.

- *Inverse flow modeling using joint geophysical and hydrological data*: This is our last attempt which is presented in the third paper. However, more studies need to be done to be able to use joint geophysical and hydrological data more efficiently in the inverse flow modeling. The main challenge is perhaps to define the weights of different types of data in a way that the final flow estimates can produce all types of data within acceptable range of uncertainties.

5 REFERENCES

Alharthi, A., and J. Lange. 1987. Soil water saturation: Dielectric determination. *Water Resour. Res*. 23(4):591-595.

Alumbaugh, D., P.Y. Chang, L. Paprocki, J.R. Brainard, R.J. Glass, and C.A. Rautman. 2002. Estimating moisture contents in the vadose zone using cross-borehole ground penetrating radar: A study of accuracy and repeatability. *Water Resour. Res.* 38:1309.

Annan, A. P. 2005. GPR methods for hydrological studies. Hydrogeophysics. Y. Rubin and S. Hubbard (Eds). 7:185-214. Springer. New York.

Binley, A., P. Winship, R. Middleton, M. Pokar and J. West. 2001. High resolution characterization of vadose zone dynamics using cross-borehole radar. *Water Resour. Res.*, 37(11), 2639-2652.

Binley, A., G. Cassiani, R. Middleton, and P. Winship. 2002. Vadose zone flow model parameterization using cross-borehole radar and resistivity imaging. *Journal of Hydrology, 267*, 147-159.

Binley, A., P. Winship, L.J. West, M. Pokar and R.Middleton. 2002. Seasonal Variation of Moisture Content in Unsaturated Sandstone Inferred from Borehole Radar and Resistivity Profiles, *J. Hydrol.*, 267(3 - 4), 160-172.

Binley, A., and K. Beven .2003. Vadose zone flow model uncertainty as conditioned on geophysical data, *Ground Water. 41*, 119-127.

Björk, A. 1996. Numerical methods for least squares problems. *Society of Industrial and Applied Mathematics*. Philadelphia, PA.

Bradford, J.H.. 2006. Applying reflection tomography in the post-migration domain to multi-fold ground-penetrating radar data. *Geophysics,* 71, K1-K8.

Brooks, R. H., and A. T. Corey. 1966. Properties of porous media affecting fluid flow. *J. Irrig. Drainage Div.*, ASCE Proc., 72 (IR2).

Carrera, J.; Neuman, S.P. 1986a: Estimation of aquifer parameters under transient and steady state conditions, 1, Maximum likelihood method incorporating prior information. *Water Resour. Res.* 22, 199–210.

Carrera, J.; Neuman, S.P. 1986b: Estimation of aquifer parameters under transient and steady state conditions, 2, Uniqueness, stability, and solution algorithms. *Water Resour. Res.* 22, 211–227.

Carrera, J.; Neuman, S.P. 1986c: Estimation of aquifer parameters under transient and steady state conditions, 3, Application to synthetic and field data. *Water Resour. Res.* 22, 228–242.

Causse, E., and P. Senechal. 2006. Model-based automatic dense velocity analysis of GPR field data for the estimation of soil properties. *J. Geophysics Eng.* 3:169-176.

Cerveny, V. 2001. Seismic rays and travel times. Page 99-228. Seismic Ray Theory. *Cambridge University Press*.

Day-Lewis, F., J. Harris, and S. Gorelick. 2002. Time-lapse inversion of crosswell radar data. *Geophysics*, 69, 1740–1752.

Day-Lewis, F. D., and J. W. Lane Jr. 2004. Assessing the resolution-dependent utility of tomograms for geostatistics, *Geophys. Res. Lett.*, *31*, L07503, doi:10.1029/2004GL019617.

Day-Lewis, F. D., K. Singha, and A. M. Binley. 2005. Applying petrophysical models to radar travel time and electrical resistivity tomograms: Resolution-dependent limitations, *J. Geophys. Res., 110*, B08206, doi:10.1029/2004JB003569.

Eppstein, M.J., and Dougherty, D.E. 1998. Efficient three-dimensional data inversion: Soil characterization and moisture monitoring from cross well GPR at a Vermont test site. *Water Resources Research*, 34(8):1889-1900.

Greaves RJ, Lesmes DP, Lee JM, Toksoz MN. 1996. Velocity variation and water content estimated from multi-offset, ground-penetrating radar. *Geophysics,* 61: 683–695.

Hanafy, S., and S.A. al Hagrey. 2006. Ground penetrating radar tomography for soil moisture heterogeneity. *Geophysics,* 71:9-18.

Hammon, W.S., X. Zeng, R.M. Corbeanu, and G.A. McMechan. 2002. Estimation of the spatial distribution of fluid permeability from surface and tomographic GPR data and core, with a 2-D example from the Ferron sandstone, Utah. *Geophysics,* 67:1505-1515.

Hubbard, S.S., J.E. Peterson, Jr., E.L. Majer, P.T. Zawislanski, K.H. Williams, J. Roberts, and F. Wobber. 1997. Estimation of permeable pathways and water content using tomography radar data. Leading Edge Explor. 16:1623-1630.

Hubbard, S., and Y. Rubin. 2000. Hydrogeological parameter estimation using geological data: A review of selected techniques. *J. Contam. Hydrol., 45,* 3–34.

Hubbard, S., K. Grote and Y. Rubin. 2002. Mapping the volumetric soil water content of a California vineyard using high-frequency GPR ground wave data, Geophysics. *The Leading Edge, Society of Exploration Geophysics,* Vol. 21 (6), pp. 552-559.

Huisman, J.A., J.J.J.C. Snepvangers, W. Bouten, and G.B.M. Heuvelink. 2003. Monitoring temporal development of spatial soil water content variation: Comparison of ground penetrating radar and time domain reflectometry. *Vadose Zone J.* 2:519-529.

Huisman, J.A., S.S. Hubbard, J.D. Redman, and A.P. Annan, 2003. Measuring soil water content with ground penetrating radar: A review. *Vadose Zone J.* 2:476-491.

Hyndman, D. W., J. M. Harris, and S. M. Gorelick. 1994. Coupled seismic and tracer inversion for aquifer property characterization, *Water Resour. Res., 30,* 1965-1977.

Hyndman, D. W., and S. M. Gorelick. 1996. Estimating lithologic and transport properties in three dimensions using seismic and tracer data: The Kesterson aquifer. *Water Resour. Res., 32*, 2659-2670.

Irving, J. D., and R. J. Knight. 2005. Effect of antennas on velocity estimates obtained from crosshole GPR data. *Geophysics*, 70(5):k39-k42.

Keers, H., L.R. Johnson, and D.W. Vasco. 2000. Acoustic cross well imaging using asymptotic waveforms. *Geophysics,* 65, 1569-1582.

Kitterød, N-O. and S. Finsterle. 2004. Simulating unsaturated flow fields based on saturation measurements. *Journal of Hydraulic Research, 42*, 121-129.

Kline, M., and I.W. Kay. 1965. Electromagnetic theory and geometrical optics. *JohnWiley & Sons. Inc.*

Kowalsky, M. B., S. Finsterle, and Yoram Rubin. 2004. Estimating flow parameter distributions using ground penetrating radar and hydrological measurements during transient flow in the vadose zone. *Advances in Water Resources.,* 27(6), 583-599.

Kowalsky, M.B., S. Finsterle, J. Peterson, S. Hubbard, Y. Rubin, E. Majer, A. Ward, and G. Gee. 2005. Estimation of field-scale soil hydraulic and dielectric parameters through joint inversion of GPR and hydrological data. *Water Resour. Res.,* 41, W11425, doi:10.1029/2005WR004237.

Lambot, S., M. Antoine, I. van den Bosch, E. C. Slab, and M. Vanclooster. 2004. Electromagnetic inversion of GPR signals and subsequent hydrodynamic inversion to estimate effective vadose zone hydraulic properties. *Vadose Zone J.,* 3:1072-1081.

Lambot, S., M. Antoine, M. Vanclooster, and E. C. Slob. 2006. Effect of soil roughness on the inversion of off-ground monostatic GPR signal for noninvasive quantification of soil properties, *Water Resour. Res.*, *42*, W03403, doi:10.1029/2005WR004416.

Linde, N., S. Finsterle, and S. Hubbard. 2006a. Inversion of tracer test data using tomographic constraints. *Water Resour. Res.,* 42, W04410, doi:10.1029/2004WR003806.

Linde, N., A. Binley, A. Tryggvason, L. B. Pedersen, and A. Revil. 2006b. Improved hydrogeophysical characterization using joint inversion of cross-hole electrical resistance and ground-penetrating radar traveltime data, *Water Resour. Res.*, *42*, W12404, doi:10.1029/2006WR005131.

Moysey, S., K. Singha, and R. Knight. 2005. A framework for inferring field-scale rock physics relationships through numerical simulation, *Geophys. Res. Lett.*, *32*, L08304, doi:10.1029/2004GL022152.

Musil, M., H. R. Maurer, and A. G. Green. 2003: Discrete tomography and joint inversion for loosely connected or unconnected physical properties: application to crosshole seismic and georadar data sets, *Geophys. J. Intern.*, 153, 389-402.

Nolet, G. 1987. Seismic tomography with application in global seismology and exploration geophysics. 1:1-18. *D. Reidel publishing Company*. Holland.

Parkin, G., D. Redman, P.B. Bertoldi, and Z. Zhang. 2000. Measurement of soil water content below a wastewater trench using ground-penetrating radar. *Water Resour. Res.* 36:2147-2154.

Persson, M., B. Sivakumar, and R. Berndtsson, O.H. Jacobsen, and P. Schjønning. 2002. Predicting the dielectric constant-water content relationship using artificial neural networks. *Soil Sci. Soc. Am. J.,* 66:1424-1429.

Ponizovsky, A.A., S.M. Chudinova, Y.A.Pachepsky. 1999. Performance of TDR calibration models as affected by soil texture. *Journal of Hydrology,* 218:35-43.

Press, H.P., S.A. Teukolsky, W.T. Vetterling, and B.P. Flannery. 1992. Numerical recipes in C: The art of scientific computing. 2-3:32-123. *Cambridge University Press*.

Roth, K. R., R. Schulin, H. Fluhler, and W. Attinger , 1990, Calibration of time domain reflectometry for water content measurement using a composite dielectric approach, *Water Resour. Res.*, Vol.26, P:2267-2273.

Rubin, Y., and S. S. Hubbard. 2005. Hydrogeophysics. *Springer*.

Rucker, D.F., and T.P.A. Ferré. 2004. Correcting water content measurement errors associated with critically refracted first arrivals on zero offset profiling borehole ground penetrating radar profiles. *Vadose Zone J.* 3:278-287.

Schmalholz, J., H. Stoffregen, A. Kemna, and U. Yaramanci. 2004. Imaging of water content distribution inside a lysimeter using GPR tomography. *Vadose Zone J.* 3:1106-1115.

Stengel, R.F. 1994. Optimal control and estimation. *Dover Publications Inc.* Mineola, New York.

Topp, G.C., J. L. Davis, , and A.P. Annan. 1980. Electromagnetic determination of soil water content: measurements in coaxial transmission lines. *Wat. Resour. Res.* 16:574-582.

Tronicke, J., K. Holliger, W. Barrash, and M. D. Knoll. 2004. Multivariate analysis of cross-hole georadar velocity and attenuation tomograms for aquifer zonation, *Water Resour. Res.*, *40*, W01519, doi:10.1029/2003WR002031.

Van Genuchten, M. Th., 1980. A closed-form equation for predicting the hydraulic conductivity of unsaturated soils. *Soil Sci. Soc. Am. J.,* 44, 892-898.

Watanabe, T., Hirai, t., & Sassa, K., 1996. Seismic traveltime tomography in anisotropic heterogeneous media, *J. Appl. Geophys.*, **35**, 133–143.

West, L. J., K. Handley, Y. Huang, and M. Pokar. 2003. Radar frequency dielectric dispersion in sandstone: Implications for determination of moisture and clay content, *Water Resour. Res.*, *39*(2), 1026, doi:10.1029/2001WR000923.

Wharton, R.P., G.A. Hazen, R.N. Rau, and D.L. Best. 1980. Electromagnetic propagation logging. Advances in Technique and Interpretation. 55th Annual Technical Conference. Paper SPE 9267. *Society of Petroleum Engineers of AIME, Richardson*, TX.

Yu, C., A. W. Warrick, M. H. Conklin, M. H. Young, and M. Zreda. 1997. Two- and three-parameter calibrations of time domain reflectometry for soil moisture measurement, *Water Resour. Res.*, 33(10), 2417–2422.

6 SUMMARY OF PAPERS

Paper I

Time Lapse GPR Tomography of Unsaturated Water Flow in an Ice-Contact Delta

M. Bagher Farmani, Henk Keers, Nils-Otto Kitterød

In this paper volumetric soil water content distribution in the vadose zone is estimated using tomography and a petrophysical relationship.

Cross well Ground Penetrating Radar (GPR) data sets were collected in the vadose zone of an ice-contact delta near Oslo's Gardermoen airport (Norway) before, during and after snowmelt in 2005. The observed travel times were inverted using curved ray travel time tomography. The tomograms are in good agreement with the local geological structure of the delta. The tomographic results are confirmed independently by surface GPR reflection data and X-ray images of core samples. In addition to structure, the GPR tomograms also show a strong time dependency due to the snowmelt. The time lapse tomograms were used to estimate volumetric soil water content using Topp's equation. The geological structure and water content estimates obtained from the GPR tomography are used in the inverse flow modeling presented in the second paper. In this paper, the water balance in the vadose zone was also calculated using snow accumulation data, precipitation data, porosity estimates and observed changes in the groundwater table. The amount of water stored in the vadose zone obtained from the water balance was consistent with the amount estimated using GPR tomography.

Paper II

Inverse Modeling of Unsaturated Flow Parameters Using Dynamic Geological Structure Conditioned by GPR Tomography

M. Bagher Farmani, Nils-Otto Kitterød, Henk Keers

This paper is the core of this study. In this paper, an inverse flow modeling method is presented to estimate the flow parameters and calibrate the geological structure of the

vadose zone conditioned on volumetric soil water content distribution. Volumetric soil water content is estimated using the method presented in the first paper and is used as constraints in the flow inversion. The influence of the tomographic artifacts on the flow inversion is minimized by assigning weights that are proportional to the ray coverage. The geological structure is defined using a set of control points, the positions of which can be modified during the inversion. After the inversion, the final geological and flow model are used to compute GPR travel times to check the consistency between these computed travel times and the observed travel times.

The method is first tested on two synthetic models (a steady state and a transient flow models). Subsequently, the method is applied to characterize the vadose zone at Oslo's Gardermoen Airport, in Norway during the snowmelt of 2005. The flow inversion method is applied to locate and quantify the main geological layers at the site. In particular the inversion method identifies and estimates the location and properties of thin dipping layers with relatively low-permeability. The flow model is cross validated using an independent infiltration event.

Paper III

Estimation of Unsaturated Flow Parameters using GPR Tomography and Groundwater Table Data

M. Bagher Farmani, Nils-Otto Kitterød, Henk Keers

In this paper the method presented in the second paper is extended to include the groundwater water table data as constrains in the flow inversion.

Flow parameters in the vadose zone of an ice-contact delta near Oslo's Gardermoen airport (Norway) are estimated by combining time-lapse Ground Penetrating Radar (GPR) travel time tomography; groundwater table data, and inverse flow modeling. Natural water infiltration into the vadose zone from the snowmelt in 2006 is used to estimate the flow parameters.

The inverse flow modeling is done by conditioning on different data sets: (1) time-lapse GPR travel time tomography; (2) groundwater table; (3) time-lapse GPR travel time

tomography and groundwater table: (4) #2, but with using an extended search space for the intrinsic permeability and van Genuchten parameter α.

The flow parameters estimated by inversion #1 capture development of the wet front, but fail to simulate the groundwater table. The flow parameters estimated by inversion #2 does not simulate the wet front correctly, but decrease the objective function better than inversion #1. When inversion is conditioned on both types of data (#3), the final estimates of the flow parameters are close to the estimates from the inversion conditioned on only groundwater table data. This happens because much denser groundwater table data are available in time than the GPR data. Finally we do forward flow modeling with the estimated parameter sets and compare the results with an independent tracer experiment performed at the field site in 1999. The results show that anisotropy in the intrinsic permeability is an important parameter which should be taken into account to be able to simulate the water paths. However, volumetric soil water content distribution is not strongly related to the anisotropy of intrinsic permeability. Therefore, anisotropy can not be correctly estimated by inverse flow modeling conditioned on volumetric soil water content only.